



Incorporating a Piperidinyl Group in the Fluorophore Extends the Fluorescence Lifetime of Click-Derived Cyclam-Naphthalimide Conjugates

Mingfeng Yu¹, Sandra Ast¹, Qun Yu¹, Anthony T. S. Lo¹, Roman Flehr², Matthew H. Todd^{1*}, Peter J. Rutledge^{1*}

¹ School of Chemistry, The University of Sydney, Sydney, New South Wales, Australia, ² Institute for Chemistry, University of Potsdam, Potsdam, Brandenburg, Germany

Abstract

Ligands incorporating a tetraazamacrocycle receptor, a 'click'-derived triazole and a 1,8-naphthalimide fluorophore have proven utility as probes for metal ions. Three new cyclam-based molecular probes are reported, in which a piperidinyl group has been introduced at the 4-position of the naphthalimide fluorophore. These compounds have been synthesized using the copper(I)-catalyzed azide-alkyne Huisgen cycloaddition and their photophysical properties studied in detail. The alkylamino group induces the expected red-shift in absorption and emission spectra relative to the simple naphthalimide derivatives and gives rise to extended fluorescence lifetimes in aqueous buffer. The photophysical properties of these systems are shown to be highly solvent-dependent. Screening the fluorescence responses of the new conjugates to a wide variety of metal ions reveals significant and selective fluorescence quenching in the presence of copper(II), yet no fluorescence enhancement with zinc(II) as observed previously for the simple naphthalimide derivatives. Reasons for this different behaviour are proposed. Cytotoxicity testing shows that these new cyclam-triazole-dye conjugates display little or no toxicity against either DLD-1 colon carcinoma cells or MDA-MB-231 breast carcinoma cells, suggesting a potential role for these and related systems in biological sensing applications.

Citation: Yu M, Ast S, Yu Q, Lo ATS, Flehr R, et al. (2014) Incorporating a Piperidinyl Group in the Fluorophore Extends the Fluorescence Lifetime of Click-Derived Cyclam-Naphthalimide Conjugates. PLoS ONE 9(7): e100761. doi:10.1371/journal.pone.0100761

Editor: A Ganesan, University of East Anglia, United Kingdom

Received: March 7, 2014; **Accepted:** May 28, 2014; **Published:** July 1, 2014

Copyright: © 2014 Yu et al. This is an open-access article distributed under the terms of the Creative Commons Attribution License, which permits unrestricted use, distribution, and reproduction in any medium, provided the original author and source are credited.

Funding: This work was supported by the National Breast Cancer Fund (<http://www.nbcf.org.au/>) with Novel Concept Grant NC-10-69, the Australian Research Council (<http://www.arc.gov.au/>) with Discovery Project Grant DP120104035, and the University of Sydney, with a University of Sydney International Scholarship (USydis) to Mingfeng Yu. The funders had no role in study design, data collection and analysis, decision to publish, or preparation of the manuscript.

Competing Interests: The authors confirm that co-author Matthew Todd is a PLOS ONE Editorial Board member. This does not alter the authors' adherence to PLOS ONE Editorial policies and criteria.

* Email: peter.rutledge@sydney.edu.au (PJR); matthew.todd@sydney.edu.au (MHT)

Introduction

Given the various essential roles played by metal ions in biological systems and environmental processes, the development of fluorescent probes with high selectivity and sensitivity for these species is of great importance. [1–8] Due to their tunable photophysical properties and ease of preparation, 1,8-naphthalimide derivatives are commonly used as fluorophores in metal ion probes. [9–22] Structural modifications of the 1,8-naphthalimide are readily accommodated on either the aromatic naphthalene moiety or the imide-NH site.

We have recently developed a novel class of fluorescent probes for Zn²⁺ (Figure 1) by attaching the 1,8-naphthalimide fluorophore to a tetraazamacrocycle scaffold *via* copper(I)-catalyzed azide-alkyne Huisgen cycloaddition (colloquially known as the click reaction). [19–22] The click-generated triazole is a linker but also acts as a coordination site, thus playing a role in the metal ion binding and detection. Compounds **1–4** signal the binding of Zn²⁺ to the tetraazamacrocycle-triazole moiety with a multifold increase in fluorescence emission of the pendant 1,8-naphthalimide. Reversing the triazole topology in the cyclam-triazole-naphthalimide system (**3** *vs.* **1**) gives a 10-fold brighter fluorescence response to Zn²⁺ in HEPES buffer (10 mM, pH 7.4). [22] Furthermore, the cyclam-based probe **1** has been used to detect the cellular Zn²⁺

flux during apoptosis *in vitro*, [21] and the cyclen-based probe **2** has been applied *in vivo* to image Zn²⁺ in zebrafish. [19] In a related approach, tethering a second pendant group (biotin) to the zinc(II) complex of compound **1** afforded a fluorescent 'allosteric scorpionand' probe **5** that visualizes the binding of the pendant biotin to the cognate biomolecule avidin. [23] Replacement of the 1,8-naphthalimide dye in compounds **1** and **3** with the coumarin fluorophore provided probes **6** and **7** (Figure 1) that respond selectively to Cu²⁺ and Hg²⁺ [22,24].

To minimize cell damage and interference from background autofluorescence in cell-based assays, the absorption and emission spectra of the fluorescent probe should be as close as possible to the red end of the visible spectrum. [25] In this regard the spectral characteristics of probes **1–7** are sub-optimal ($\lambda_{\text{abs}} \sim 320\text{--}360$ nm, $\lambda_{\text{em}} \sim 380\text{--}460$ nm in aqueous buffer). [19–24] Previous studies have shown that introducing alkylamino groups at the naphthalene moiety of 1,8-naphthalimide induces such a bathochromic shift. [11,26–29] To this end, we designed three new cyclam-piperidinyl-naphthalimide conjugates **8–10** (Figure 2). A phenyl linker was used in compounds **8** and **10** to connect the cyclam-triazole moiety to the piperidinyl-naphthalimide fluorophore, while compound **9**, containing a flexible ethylene chain, was designed as a control to verify the importance of conjugation. The metal-ion

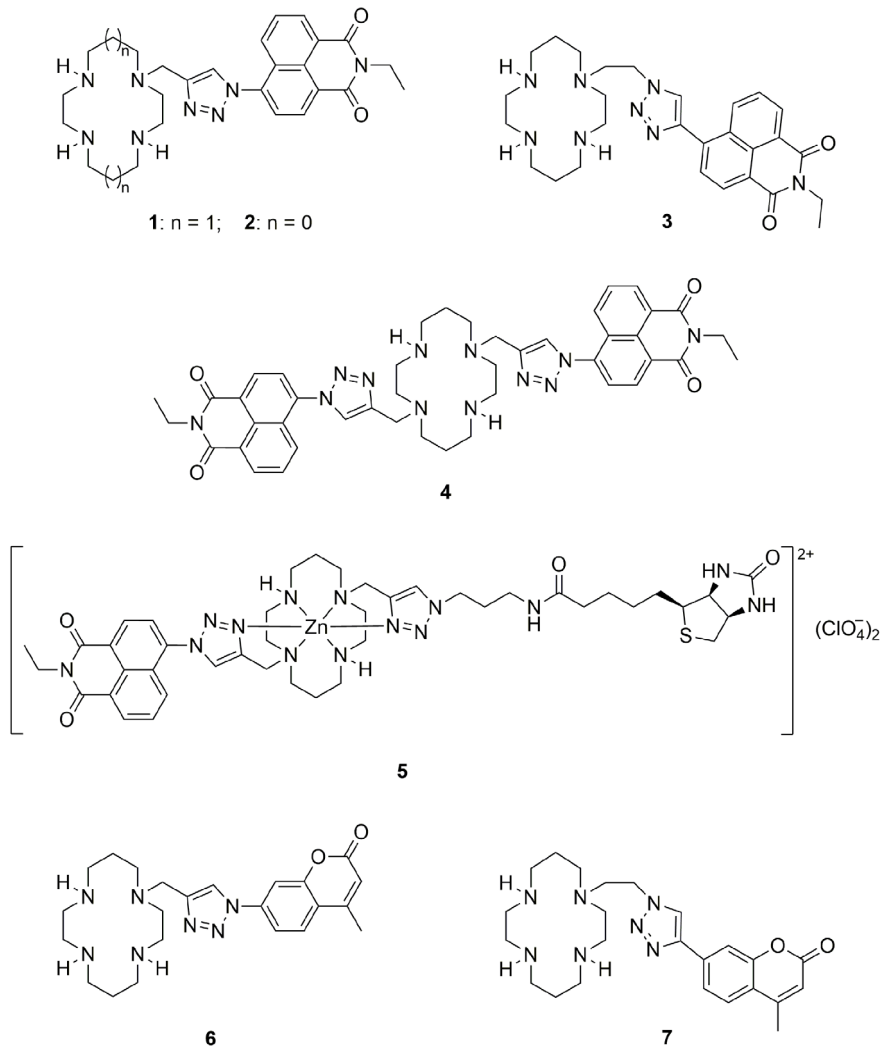


Figure 1. Fluorescent probes 1–7 used in previous studies.

doi:10.1371/journal.pone.0100761.g001

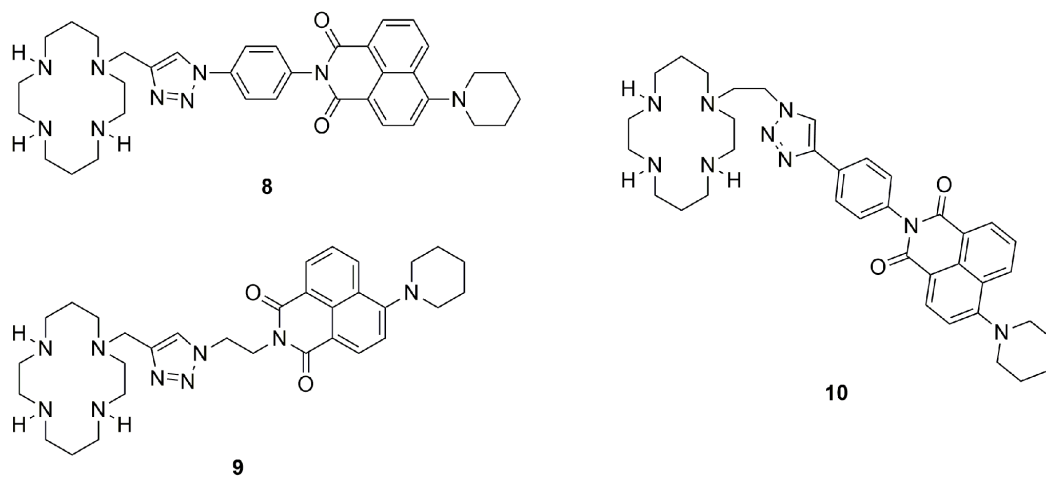


Figure 2. Cyclam-piperidinyl-naphthalimide conjugates 8–10 studied in this work.

doi:10.1371/journal.pone.0100761.g002

responsiveness, fluorescence quantum yields and decay times, and cytotoxicity of these new conjugates were investigated to explore their potential for application as metal ion probes *in vitro* and *in vivo*.

Results and Discussion

(a) Synthesis

Synthesis of the cyclam-piperidinyl-naphthalimide conjugates **8–10** required the preparation of precursors **13**, **17** and **20** (Figure 3). Azide **17** [30,31] and alkyne **20** [29,30,32] were successfully synthesized according to literature procedures, whereas the preparation of azide **13** proved challenging. Conversion of bromide **12** to the corresponding azide **13** was initially attempted with sodium azide in the presence of sodium ascorbate, copper(I) iodide and *N,N'*-dimethylethylenediamine (DMEDA) at reflux in either an ordinary round-bottomed flask or a pressure tube. [33–35] A solvent screen including methanol/water, ethanol/water or dimethyl sulfoxide (DMSO)/water (7:3 in all cases) failed to afford the desired azide **13**, giving instead full recovery of starting material **12**; this outcome may be attributed to the extraordinarily low solubility of bromide **12** in these solvent combinations. Switching to tetrahydrofuran (THF)/water (7:3), all reactants and reagents were dissolved at reflux in the pressure tube and reaction proceeded to give azide **13** in 50% yield. The corresponding amine was also detected by LCMS analysis of the reaction mixture, consistent with previous observations that both azide and amine may be generated through a copper-assisted aromatic substitution reaction with sodium azide. [33] Reacting each of the three precursors **13**, **17** and **20** individually with the complementary propargyl-tri-Boc cyclam [23,36] or azidoethyl-tri-Boc cyclam [24] under standard click conditions [24,36] yielded the Boc-protected cyclam-piperidinyl-naphthalimide conjugates **14**, **18** and **21** respectively in good to excellent yields. Removal of Boc groups from these conjugates was effected in a mixture of TFA/DCM/H₂O (90:5:5), [23,36,37] followed by basification to recover the corresponding free amines **8–10**. However, the outcome of the basification step was contingent on the base used. Addition of 2 M sodium hydroxide solution [36,38] or saturated sodium carbonate solution [36] resulted in decomposition of the desired free amines or incomplete removal of trifluoroacetate counter ions respectively (indicated by analysis with ¹H and ¹³C NMR spectroscopy). Successful isolation of the pure amines **8–10** was achieved using excess Ambersep 900 (hydroxide form) in methanol.

(b) Photophysical Properties

i) Steady-state photophysical properties. The steady state photophysical properties of cyclam-piperidinyl-naphthalimide conjugates **8–10** were investigated using both UV-Vis and fluorescence spectroscopy. The UV-Vis absorption spectra of **8–10** in HEPES buffer (10 mM, pH 7.4) are almost identical, with the lowest-energy absorption (λ_{abs}) centered at 415 ± 2 nm and stretching out to 500 nm (Figure 4). The fluorescence emission spectra of **8–10** are only slightly shifted giving a broad emission band ranging from 500 to 700 nm, centered around 545–558 nm (λ_{em}) (Figure 4). Introduction of the piperidine to the naphthalimide fluorophore not only leads to a red-shifted emission maximum but also to a broadening of both the absorption and emission bands. The similarity of these spectra in aqueous buffer is remarkable, and implies i) the role of the linker (phenyl **8** vs ethyl **9**) exerts minimal influence and ii) the triazole connectivity (**8** vs **10**) does not have a significant impact on the UV-Vis absorption and fluorescence emission of these conjugates. The fact that the π -system is not extended in **8** or **10** by conjugation of the phenyl

group with the 1,8-naphthalimide core can be rationalized by considering a twisting of the two aromatic planes to minimize adverse steric interactions. This effect may be enhanced after excitation of the probe, giving rise to charge separated states and significant solvent-dependent variation in spectral properties.

Screening the spectral properties of **8–10** in various solvents spanning a wide range of polarities revealed a solvent-dependent shift in absorption, and – to a much larger extent – emission maxima (Table 1). Comparing measurements made in aqueous buffer versus non-polar toluene shows that the impact of solvent polarity is less in the case of ethyl-linked **9**, where the emission in HEPES buffer (545 nm) shifts less than 40 nm in toluene (507 nm). In the emissions of **8** and **10**, a blue-shift of nearly 60 nm is seen in toluene relative to HEPES buffer. The Stokes shifts ($\Delta\lambda$) (calculated from the difference of the absorption and emission maxima) allow easier comparison: the Stokes shifts of ligands **8** and **10** respond similarly throughout the solvent screen; the slight differences that are observed between the two ligands can be attributed to the effect of the different triazole connectivity (further evidence for the minor impact this structural change exerts on the spectral properties). More importantly, there is a distinct decrease in the Stokes shift of both compounds when moving from HEPES buffer into less polar solvents, suggesting that charge separation in the excited state is most likely linked to conformational changes. In the ethyl-linked analogue **9**, the effect of the solvent is weaker, indicating that the excited state of **9** incorporates a much smaller charge separation. Lippert-Mataga plots [39–41] (Figures S1–S3 and Text S1 in File S1) were constructed to build a picture of solvent-fluorophore interactions. The Stokes shifts of all three conjugates in the hydrogen bonding solvents (*e.g.* alcohols) are typically greater than those in solvents that less readily form hydrogen bonds (*e.g.* toluene); such behavior can be attributed to protic solvent-fluorophore hydrogen bonding and has been observed for other fluorophores [42,43].

ii) Response to metal ions. The UV-Vis and fluorescence responses of conjugates **8–10** to a wide variety of metal ions (Ag⁺, Ba²⁺, Ca²⁺, Cd²⁺, Co²⁺, Cu²⁺, Fe²⁺, Fe³⁺, Hg²⁺, K⁺, Li⁺, Mg²⁺, Mn²⁺, Na⁺, Ni²⁺, Pb²⁺, Rb⁺ and Zn²⁺) were assessed in HEPES buffer (10 mM, pH 7.4 – see File S1). Of the metals tested, only Cu²⁺ triggered a significant response, quenching the fluorescence of all three conjugates (Figures S4–S6 in File S1). This response is consistent with previous observations that Cu²⁺ quenches the fluorescence of derivatives **1**, **3**, **6** and **7**, [20–22] and may be due to paramagnetic or heavy atom effects; [44–47] work is underway to determine the mechanism of Cu²⁺-mediated fluorescence quenching in these systems. However none of the cyclam-piperidinyl-naphthalimide conjugates **8–10** show any meaningful response to either Zn²⁺ or Hg²⁺, in contrast to the previously-reported cyclam-naphthalimide conjugates **1**, **3** and **4** which exhibited fluorescence increases in the presence of Zn²⁺ and quenching in response to Hg²⁺ respectively. [20–22] Addition of Co²⁺, Fe²⁺ and Fe³⁺ each triggered a small to moderate reduction in the fluorescence of **10**, but had no effect on the fluorescence of **8** or **9**. Taken together, these fluorescence results imply that both the nature of the pendant fluorophore and the connectivity between the fluorophore and metal-cyclam complex play a role in the metal-ion responsiveness of these conjugates. The addition of these metal ions had no significant effect on the UV-Vis absorption spectra of all three conjugates (Figures S7–S9 in File S1).

To investigate the effectiveness of **8–10** as probes for Cu²⁺ in the presence of competing metal ions, competitive binding experiments were conducted using Zn²⁺. Thus a 10 μ M solution of **8–10** in HEPES buffer (10 mM, pH 7.4) was combined with 50 equivalents of Zn²⁺, followed after approximately 3 minutes by 1

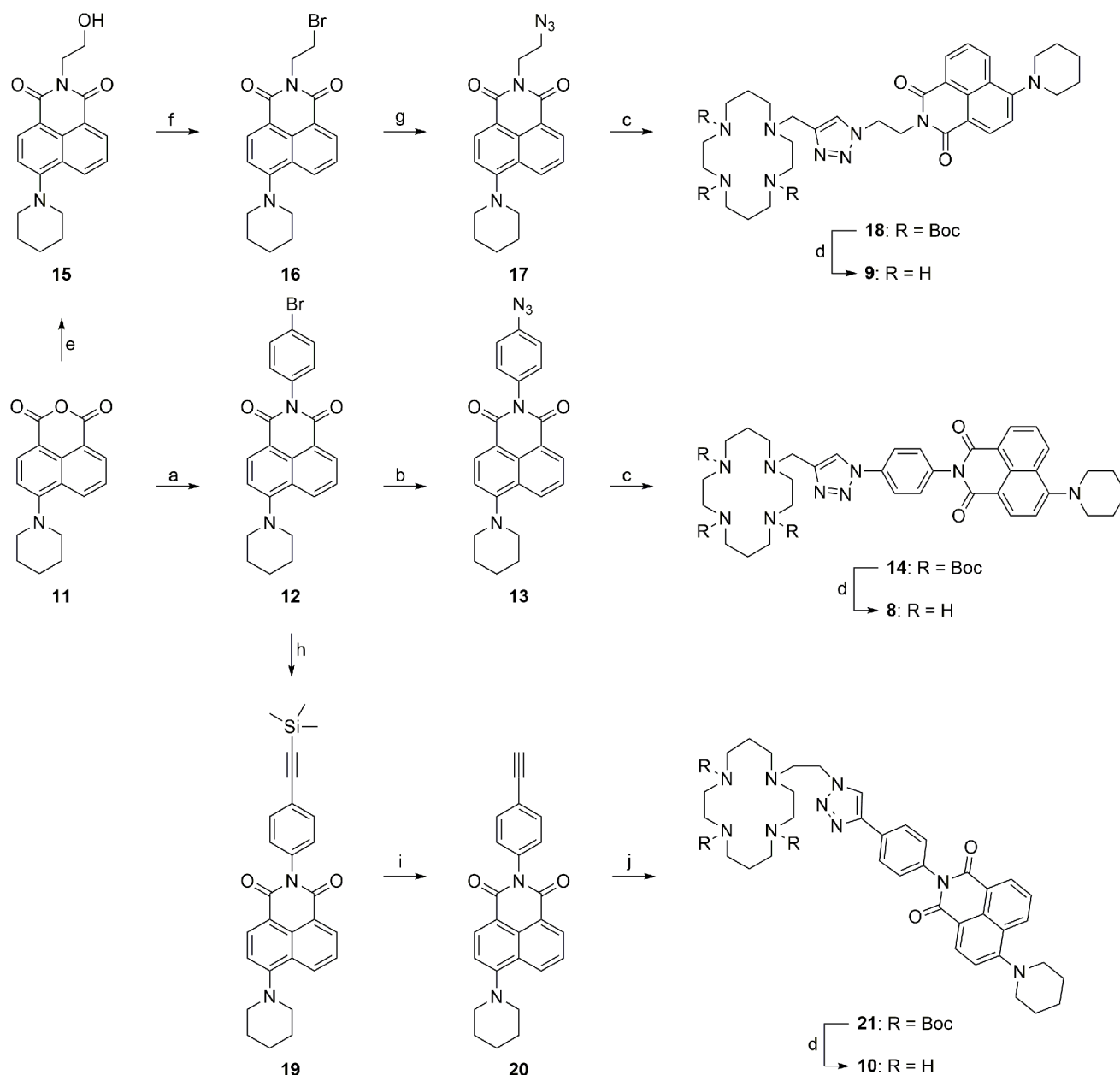


Figure 3. Synthesis of the cyclam-piperidinyl-naphthalimide conjugates 8–10. Reagents and conditions: (a) 4-bromoaniline, piperidine, 2-methoxyethanol, reflux, 72 h, 90%; (b) NaN_3 , CuI , sodium ascorbate, DMEDA, THF/ H_2O (7:3), 12 h, 50%; (c) propargyl-tri-Boc cyclam, $\text{CuSO}_4 \cdot 5\text{H}_2\text{O}$, sodium ascorbate, THF/ H_2O (7:3), rt for **13** and 50°C for **17**, 12 h, **14**: 96%, **18**: 92%; (d) (i) TFA/DCM/ H_2O (90:5:5), rt, 6 h; (ii) Ambersep 900 hydroxide form, CH_3OH , rt, 15 min, **8**: 96%, **9**: 99%, **10**: 99%; (e) 2-aminoethanol, EtOH, reflux, 22 h, 92%; (f) PBr_3 , pyridine, THF, 50°C , 16 h, 60%; (g) NaN_3 , EtOH, reflux, 6 h, 80%; (h) trimethylsilylacetylene, CuI , triphenylphosphine, $\text{Pd}(\text{PPh}_3)_4$, Et_3N , pyridine, 85°C , o/n, 94%; (i) K_2CO_3 , CH_3OH , rt, o/n, 97%; (j) 2-azidoethyl-tri-Boc cyclam, $\text{CuSO}_4 \cdot 5\text{H}_2\text{O}$, sodium ascorbate, THF/ H_2O (7:3), 12 h, 66%. doi:10.1371/journal.pone.0100761.g003

equivalent of Cu^{2+} . In all cases, much weaker fluorescence quenching was observed than in the experiments in which the two metal ions were added in the reverse order, or a premixed $\text{Cu}^{2+}/\text{Zn}^{2+}$ (1:50) solution was added (Figure 5). These results show the effectiveness of **8–10** as Cu^{2+} -probes but indicate a limitation in the presence of high Zn^{2+} concentrations.

The fluorescence responses of probes **8–10** were evaluated over a wide pH range, both in the absence and presence of Cu^{2+} (Figures S10–S12 in File S1). These experiments indicate optimum responsiveness to Cu^{2+} at neutral pH. At low pH, the fluorescence responses of the free ligands **8–10** change little in the presence of

Cu^{2+} , presumably due to inhibition of metal coordination when the cyclam amine groups are protonated. The fluorescence of the free ligands **8–10** is diminished at high pH, as previously observed with probe **1**. [21] However, it is the absence of any protonation-induced fluorescence enhancement with probes **8–10** that is more significant. This indicates that the photoinduced electron transfer (PET) from the cyclam-triazole moiety to naphthalimide observed with probes **1–3** [22] does not occur with the piperidinyl-naphthalimide fluorophore incumbent. This in turn means that the full fluorescence response of **8–10** is turned ‘on’ in the free ligands, eliminating the possibility of a fluorescence ‘turn-on’ pathway

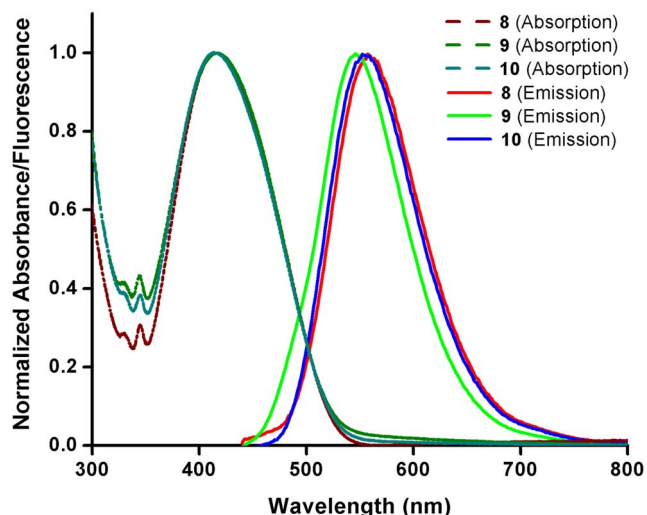


Figure 4. Normalized UV-Vis and fluorescence spectra of 8–10. Experiments were carried out in HEPES buffer (10 mM, pH 7.4) at 25°C. doi:10.1371/journal.pone.0100761.g004

upon protonation or metal binding. The fact that PET is not favoured with probes **8–10** can be rationalized by considering the push-pull-character of the 4-aminonaphthalimide, where the electron acceptor is located at the amine and the electron donor at the imide. In the excited state, the resultant negative charge density on the imide inhibits acceptance of an additional electron *via* PET when the electron donor is connected at this position on the fluorophore [48].

iii) Time resolved photophysical properties and fluorescence quantum yields. Fluorescence quantum yields were acquired in three representative solvents (HEPES buffer, ethyl acetate and acetonitrile) to investigate the intrinsic photophysical properties in more detail (Table 2). In HEPES-buffer and acetonitrile, the quantum yields and the fluorescence decay times of the free ligands **8–10** are generally low, although ligand **9** gives a significantly longer decay time ($\langle\tau\rangle = 4.86$ ns) in buffer compared to ligands **8** and **10** ($\langle\tau\rangle = 2.47$ and 2.42 ns respectively). The quantum yields in ethyl acetate (0.25–0.50) are at least one order of magnitude higher than in acetonitrile (0.036–0.052) and about twice as high as in buffer (0.005–0.009). Clearly solvent has a strong influence on the photophysical properties of these probes. Strong solvent-dependence was also observed in the decay time profile of all three ligands. In ethyl acetate, ligands **8** and **10** decay with a single exponential profile, ligand **9** with a bi-exponential profile. In acetonitrile, decay times for all three ligands are fitted with two exponentials. In buffer, three exponentials give the best fit in all three cases. These multi-exponential fits indicate the presence of multiple excited species in these solvents. The additional components observed in aqueous buffer over the organic solvents can be rationalized by considering changes in ligand protonation, which give rise to new species that are absent in the aprotic organic solvents. Interestingly, the photophysical properties of **8**, **9** and **10** change relative to each other with changes in solvent: while similar values for quantum yields and decay times are observed for all three ligands in acetonitrile, only **8** and **10** afford similar data in ethyl acetate and buffer, and the values recorded for **9** are appreciably different. In ethyl acetate, longer decay times for **8** and **10** (5.73 and 6.36 ns respectively) and higher quantum yields (0.44 and 0.50) are found compared to ligand **9**, but in buffer ligand **9** gives higher values than ligands **8** and **10**. Notably, the averaged decay of **9** is

particularly long (~ 5 ns) in the aqueous solvent. The long decay times may render these new probes suitable for time-correlated assays, *e.g.* fluorescence lifetime imaging (FLIM) techniques in biological samples.

(c) Biological Evaluation

The cytotoxicity of cyclam-piperidinyl-naphthalimide conjugates **8–10** and Boc-protected precursors **14**, **18**, and **21** was assayed against DLD-1 colon carcinoma cells and MDA-MB-231 breast carcinoma cells (Table 3). Cisplatin was used as a positive control in this cell viability study; its cytotoxicity against DLD-1 cells was found to be 11.2 ± 0.3 μ M, consistent with literature value of 11.8 ± 1.2 μ M. [49] Five of the six cyclam-piperidinyl-naphthalimide compounds did not display any significant cytotoxicity against either cell line, with a safe dosage level of 20 μ M. The single exception was conjugate **10**, which showed moderate activity against both carcinoma cell lines. In general, IC_{50} values for all cyclam-piperidinyl-naphthalimide conjugates **8–10** were lower than those for the corresponding Boc-protected counterparts **14**, **18** and **21**.

Conclusions

We have reported the synthesis of three cyclam-piperidinyl-naphthalimide conjugates **8–10** which respond to the presence of copper(II) with a significant decrease in fluorescence. Despite the different triazole connectivities and the variation of the pendant alkyl arm length, these probes exhibit remarkably similar photophysical properties. However, these photophysical properties are highly dependent on solvent, as seen in the UV-Vis and fluorescence spectra, quantum yields and decay times of all three ligands. The influence of the flexible ethyl linker is reflected in the long averaged fluorescence decay time of compound **9** in HEPES buffer, which is twice as long as those of ligands **8** and **10**. None of the probes display significant cytotoxicity to mammalian cells, supporting the potential suitability of this new probe class for sensing, labeling or imaging studies in biological systems.

Experimental

(a) General Materials

All reactions except azidation of **12** were carried out with continuous magnetic stirring in ordinary glassware; azidation of **12** was performed in a 15 mL Ace pressure tube, purchased from Sigma-Aldrich. Heating of reactions was conducted with a paraffin oil bath or a water bath. All reagents and solvents were purchased from Sigma-Aldrich, Alfa Acer, Merck, or Ajax Finechem. Reagents were used as received unless otherwise specified. Hexane and ethyl acetate were distilled before use. Dichloromethane and ethanol were distilled over calcium hydride and stored over activated 4 Å molecular sieves. Tetrahydrofuran was distilled over sodium wire/benzophenone. Methanol and acetonitrile were collected freshly from a PureSolv MD 7 solvent purification system having been passed through anhydrous alumina columns.

(b) Instrumentation and Methods

^1H and ^{13}C NMR spectra were recorded at 300 K on a Bruker AVANCE 300 spectrometer (^1H at 300.13 MHz and ^{13}C at 75.47 MHz) or a Bruker DRX 400 spectrometer (^1H at 400.13 MHz and ^{13}C at 100.61 MHz). ^1H and ^{13}C NMR spectra are referenced to ^1H signals of residual nondeuterated solvents (or tetramethylsilane) and ^{13}C signals of the deuterated solvents respectively. ^1H NMR signals are reported with chemical shift values δ (ppm), multiplicity (s = singlet, d = doublet, t = triplet,

Table 1. Photophysical properties of 8–10 in various solvents with decreasing polarity from aqueous (HEPES buffer) to toluene.

Solvent	$\lambda_{\text{abs}}/\text{nm}$			$\lambda_{\text{em}}/\text{nm}$			$\nu_{\text{max}}/\text{cm}^{-1}$		
	8	9	10	8	9	10	8	9	10
HEPES	415	417	414	558	545	555	6175	5632	6137
MeOH	415	7	415	542	538	542	5646	5393	5646
EtOH	413	415	412	540	536	539	5695	5440	5719
n-PrOH	413	413	412	537	534	536	5591	5486	5615
n-BuOH	413	411	411	536	534	534	5556	5604	5604
DMSO	415	416	413	540	536	540	5578	5382	5695
MeCN	411	412	409	539	537	538	5778	5650	5863
DMF	410	412	409	538	535	537	5803	5580	5828
Acetone	406	409	405	531	530	530	5798	5582	5823
EtOAc	401	404	398	518	520	515	5633	5522	5708
THF	403	406	401	517	518	514	5472	5326	5482
DCM	418	421	415	523	524	521	4803	4669	4903
CHCl ₃	418	418	415	513	516	512	4430	4544	4565
Toluene	404	406	402	500	507	499	4752	4907	4836

λ_{abs} : wavelength of maximum UV-Vis absorbance; λ_{em} : wavelength of maximum emission intensity; ν_{max} : Stokes shift.
doi:10.1371/journal.pone.0100761.t001

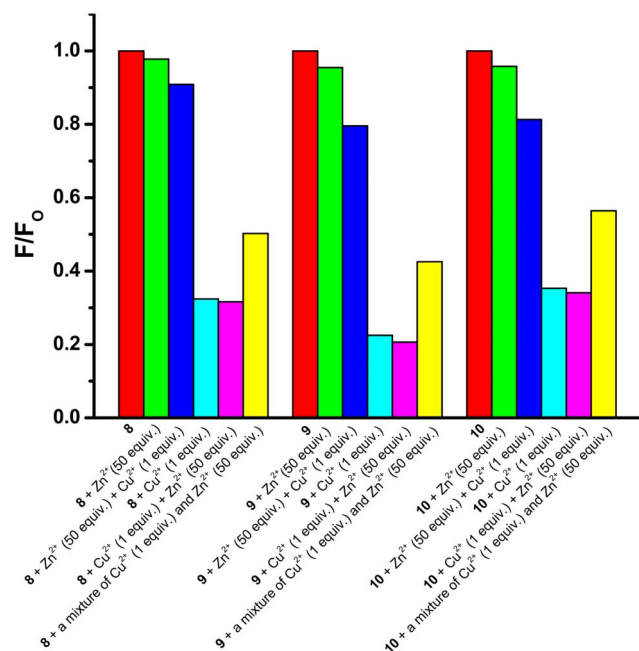


Figure 5. Competitive binding experiments. Experiments were carried out to investigate the effectiveness of Cu²⁺-induced (1 equiv.) quenching of the fluorescence of probes **8–10** (10 μM) in HEPES buffer (10 mM, pH 7.4) at 25 °C in the presence of excess Zn²⁺ (50 equiv.). doi:10.1371/journal.pone.0100761.g005

q = quartet, dd = doublet of doublets, m = multiplet and br = broad), relative integral, coupling constants J (Hz) and assignments. Infrared spectra were recorded on a Bruker Alpha FT-IR spectrometer. Low resolution and high resolution mass spectra were recorded on a Finnigan LCQ mass spectrometer and a Bruker 7T Fourier Transform Ion Cyclotron Resonance (FT-ICR) Mass Spectrometer respectively. Ionisation of all samples was carried out using either ESI or APCI. Melting points were determined on an OptiMelt 100 automated melting point apparatus and are uncorrected. Elemental analyses were carried out by the Campbell Microanalytical Laboratory (University of Otago, New Zealand) on a Carlo Erba EA 1108 Elemental Analyser. HEPES buffer was sterile filtered before use and the pH values were determined by a Mettler Toledo S20 SevenEasyTM

pH meter or Minilab ISFET pH meter. Analytical TLC was performed on Merck silica gel 60 F₂₅₄ pre-coated aluminum plates (0.2 mm) and visualized under UV light (254 nm), followed by staining with ninhydrin. Flash column chromatography was carried out using Merck silica gel 60 (0.040–0.063 mm). UV-Vis spectra were recorded on a Varian Cary 4000 or Varian Cary 1E UV-visible spectrophotometer. Fluorescence spectra were recorded on a Varian Cary Eclipse fluorescence spectrophotometer. Temperature control for both UV-visible spectrophotometer and fluorescence spectrophotometer was provided by a Varian Cary PCB water peltier system. In the time-resolved measurements, the frequency doubled output of Titan sapphire laser (Tsunami 3960; Spectra Physics) was used for excitation. The repetition rate of 80.2 MHz was reduced to 3.8 MHz with a Pulse Picker (Pulse Select; APE). The luminescence was detected in a right angle configuration to the incoming beam. For the detection, a multichannel plate (ELDI EM1-132/300; europhoton GmbH) coupled to a FL920 fluorescence lifetime spectrometer (Edinburgh Instruments) was used. The time-resolved emission was recorded in time-correlated single photon counting mode. The FAST software package (Edinburgh Instruments) was used to analyse the fluorescence decays. The fluorescence quantum yields were measured on a PL Quantum Yield Measurement System C9920-02 with an integrating sphere (Hamamatsu).

(c) Synthesis

See the Supporting Information for synthetic experimental procedures of known compounds (Text S2 and Figures S13–S15 in File S1) and ¹H and ¹³C NMR spectra of novel compounds (Figures S16–S33 in File S1).

General Synthetic Procedure A: The Copper(I)-Catalyzed Huisgen 1,3-Dipolar Cycloaddition of Azides and Alkynes. Alkyne (1.00 eq.) and azide (1.00 eq.) were dissolved in THF/H₂O (7:3, 50 mM in alkyne). A brown cloudy solution of CuSO₄·5H₂O (0.05 eq., 5 mol%) and sodium ascorbate (0.10 eq., 10 mol%) in H₂O (25 mM in copper) was added. The reaction mixture was stirred at room temperature [23,36,37] or heated at 50 °C under Ar for 12 h and quenched with saturated aqueous NH₄Cl (100 L/mol copper). THF was evaporated under reduced pressure, and the remaining mixture was extracted with DCM (3 ×). The combined organic extracts were dried over Na₂SO₄ and concentrated under reduced pressure. The residue was purified by flash column chromatography (silica gel, EtOAc:petroleum benzene = 1:1 ramping to EtOAc) to give the desired triazole.

Table 2. Fluorescence quantum yields (Φ_F) and decay times (τ) of **8–10** in HEPES buffer (10 mM, pH 7.4), ethyl acetate and acetonitrile.

Solvent	Compound	Φ_F	τ /ns	$\langle \tau \rangle$ /ns		
HEPES	8	0.005	0.12 (28%)	2.32 (46%)	5.28 (26%)	2.47
	9	0.009	0.10 (9%)	4.03 (45%)	6.60 (46%)	4.86
	10	0.005	0.17 (26%)	1.83 (37%)	4.58 (37%)	2.42
EtOAc	8	0.44	5.73			5.73
	9	0.25	2.36 (29%)	5.13 (71%)		4.33
	10	0.50	6.36			6.36
MeCN	8	0.043	0.85 (94%)	8.38 (6%)		1.30
	9	0.036	0.80 (94%)	8.58 (6%)		1.27
	10	0.052	1.04 (95%)	7.18 (5%)		1.35

$\langle \tau \rangle$ is the averaged time from the multi-exponential decay profiles.

doi:10.1371/journal.pone.0100761.t002

Table 3. Cytotoxicity of 8–10, 14, 18 and 21 against DLD-1 colon carcinoma cells and MDA-MB-231 breast carcinoma cells after incubation for 72 h.

Compound	IC ₅₀ /μM	
	DLD-1	MDA-MB-231
cisplatin	11.2±0.3	22.0±0.6
8	>100	54.1±0.8
9	>200	>100
10	53.8±1.3	37.4±0.6
14	>200	>200
18	>200	>100
21	>200	>200

IC₅₀ values are expressed as mean ± standard error of mean of at least 3 independent experiments.
doi:10.1371/journal.pone.0100761.t003

General Synthetic Procedure B: TFA-Mediated Boc Removal [23,36,37] & Basification of Trifluoroacetates. Boc-protected amine (1.0 eq.) was dissolved in a mixture of TFA/DCM/H₂O (90:5:5, 5 mM). The reaction mixture was stirred at room temperature for 6 h and concentrated under reduced pressure. The residue was dissolved in CH₃OH (5 mL), and Ambersep 900 hydroxide form (pre-swelled with H₂O for 30 min and CH₃OH for 30 min) in CH₃OH (10 mL) was added. The mixture was stirred at room temperature for 15 min and filtered, and the solid was washed with CH₃OH (15 mL). The filtrate and washings were combined and concentrated under reduced pressure to give the desired *N*-functionalized cyclam.

2-(4-Azidophenyl)-6-(piperidin-1-yl)-1*H*-benzo[de]isoquinoline-1,3(2*H*)-dione (13). To a solution of **12** (218 mg, 0.501 mmol) and sodium azide (65.0 mg, 1.00 mmol) in THF/H₂O (7 mL/3 mL) in an Ace pressure tube were added CuI (19 mg, 0.10 mmol), sodium ascorbate (10 mg, 0.050 mmol) and DMEDA (22 μL, 0.20 mmol). The reaction mixture was heated at reflux under Ar for 12 h and cooled to room temperature. After addition of H₂O (7 mL), the reaction mixture was extracted with DCM (3×25 mL). The combined organic extracts were concentrated under reduced pressure, and the residue was purified by flash column chromatography (silica gel, DCM) to give **13** as a yellow solid (100 mg, 50%). **R_F** (DCM) 0.66. **m.p.** 190–191°C. **IR** ν_{\max} /cm⁻¹ 2936, 2853, 2794, 2112, 1705, 1657, 1589, 1506, 1452, 1375, 1287, 1234, 1195, 1143. **¹H NMR** (300 MHz, CDCl₃) δ 1.60–1.84 (m, 2H, CH₂CH₂CH₂CH₂CH₂), 1.84–2.10 (m, 4H, CH₂CH₂CH₂CH₂CH₂), 3.26 (t, 4H, *J* 5.1, CH₂NCH₂), 7.18 (d, 2H, *J* 8.4, Ph-H), 7.19 (d, 1H, *J* 7.5, naphthalene-H), 7.30 (d, 2H, *J* 8.7, Ph-H), 7.70 (t, 1H, *J* 7.8, naphthalene-H), 8.43 (d, 1H, *J* 8.4, naphthalene-H), 8.51 (d, 1H, *J* 8.1, naphthalene-H), 8.59 (d, 1H, *J* 7.5, naphthalene-H). **¹³C NMR** (75 MHz, CDCl₃) δ 24.4, 26.3, 54.6, 114.9, 115.7, 120.0, 123.2, 125.5, 126.4, 130.3, 130.4, 131.2, 131.6, 132.5, 133.3, 140.2, 157.8, 164.3, 164.8 (four carbon signals overlapping or obscured). **HRMS** (ESI) 420.14297 ([M+Na]⁺); calcd. for C₂₃H₁₉N₅NaO₂ ([M+Na]⁺) 420.14310.

Tri-tert-butyl 11-((1-(4-(1,3-dioxo-6-(piperidin-1-yl)-1*H*-benzo[de]isoquinolin-2(3*H*)-yl)phenyl)-1*H*-1,2,3-triazol-4-yl)methyl)-1,4,8,11-tetraazacyclotetradecane-1,4,8-tricarboxylate (14). Propargyl-tri-Boc cyclam [23,36] (84 mg, 0.16 mmol) and azide **13** (62 mg, 0.16 mmol) were reacted at room temperature using general synthetic procedure A to give **14** as a yellow foam (140 mg, 96%). **R_F** (EtOAc:hexane = 1:1) 0.19. **IR** ν_{\max} /cm⁻¹ 2973, 2934, 2857, 2816, 1670, 1584, 1517, 1460, 1413, 1365, 1322, 1298, 1234, 1160, 1075, 1039, 995, 915, 857, 832. **¹H**

NMR (300 MHz, CDCl₃) δ 1.44 (s, 9H, C(CH₃)₃), 1.46 (s, 18H, 2×C(CH₃)₃), 1.70–1.85 (m, 4H, CH₂CH₂CH₂CH₂CH₂ & NCH₂CH₂CH₂N), 1.85–2.02 (m, 6H, CH₂CH₂CH₂CH₂CH₂ & NCH₂CH₂CH₂N), 2.45–2.60 (m, 2H, CH₂N(CH₂-triazole)CH₂), 2.62–2.78 (m, 2H, CH₂N(CH₂-triazole)CH₂), 3.28 (t, 4H, *J* 4.8, CH₂N(naphthalene)CH₂), 3.20–3.54 (m, 12H, 3×CH₂N(Boc)CH₂), 3.91 (s, 2H, NCH₂-triazole), 7.22 (d, 1H, *J* 8.1, naphthalene-H), 7.49 (d, 2H, *J* 8.7, Ph-H), 7.72 (t, 1H, *J* 7.8, naphthalene-H), 7.96 (d, 2H, *J* 8.4, Ph-H), 8.08 (br s, 1H, triazole-H), 8.46 (d, 1H, *J* 8.4, naphthalene-H), 8.54 (d, 1H, *J* 8.1, naphthalene-H), 8.62 (d, 1H, *J* 7.2, naphthalene-H). **¹³C NMR** (75 MHz, CDCl₃) δ 24.4, 26.3, 28.6, 45.7, 47.4, 48.9, 51.4, 54.6, 79.7, 114.9, 115.6, 121.2, 123.1, 125.5, 126.4, 130.5, 131.4, 131.6, 133.3, 136.0, 136.9, 144.4, 155.6, 155.9, 157.9, 164.1, 164.7 (twenty four carbon signals overlapping or obscured). **MS** (ESI) *m/z* 936.0 ([M+H]⁺, 48%), 958.1 ([M+Na]⁺, 100%). **HRMS** (ESI) 936.53398 ([M+H]⁺); calcd. for C₅₁H₇₀N₉O₈ ([M+H]⁺) 936.53419.

2-(4-(4-((1,4,8,11-Tetraazacyclotetradecan-1-yl)methyl)-1*H*-1,2,3-triazol-1-yl)phenyl)-6-(piperidin-1-yl)-1*H*-benzo[de]isoquinoline-1,3(2*H*)-dione (8). Compound **14** (112 mg, 0.120 mmol) was deprotected using general synthetic procedure B to give **8** as a yellow glue (73 mg, 96%). **IR** ν_{\max} /cm⁻¹ 3384, 3287, 3123, 3058, 2926, 2850, 2820, 1701, 1660, 1584, 1517, 1457, 1367, 1233, 1189, 1135, 1114, 1078, 1044, 998, 833. **¹H NMR** (400 MHz, CDCl₃) δ 1.56–1.81 (m, 4H, CH₂CH₂CH₂CH₂CH₂ & NCH₂CH₂CH₂N), 1.81–2.10 (m, 6H, CH₂CH₂CH₂CH₂CH₂ & NCH₂CH₂CH₂N), 2.40–3.10 (m, 19H, 3×CH₂NHCH₂ & CH₂N(CH₂-triazole)CH₂), 3.15–3.40 (m, 4H, CH₂N(naphthalene)CH₂), 3.93 (s, 2H, NCH₂-triazole), 7.20 (d, 1H, *J* 8.0, naphthalene-H), 7.47 (d, 2H, *J* 8.4, Ph-H), 7.70 (t, 1H, *J* 8.0, naphthalene-H), 7.92 (d, 2H, *J* 8.4, Ph-H), 8.11 (s, 1H, triazole-H), 8.44 (d, 1H, *J* 8.4, naphthalene-H), 8.51 (d, 1H, *J* 8.0, naphthalene-H), 8.58 (d, 1H, *J* 7.2, naphthalene-H). **¹³C NMR** (100 MHz, CDCl₃) δ 24.3, 26.1, 28.8, 46.9, 47.1, 48.0, 48.8, 49.3, 49.5, 50.7, 52.9, 54.5, 54.7, 114.7, 115.3, 120.8, 121.0, 122.9, 125.4, 126.3, 130.3, 130.4, 131.2, 131.5, 133.2, 135.8, 136.9, 145.0, 157.8, 163.9, 164.5 (five carbon signals overlapping or obscured). **MS** (ESI) *m/z* 636.3 ([M+H]⁺, 100%). **HRMS** (ESI) 636.37673 ([M+H]⁺); calcd. for C₃₆H₄₆N₉O₂ ([M+H]⁺) 636.37690.

Tri-tert-butyl 11-((1-(2-(1,3-dioxo-6-(piperidin-1-yl)-1*H*-benzo[de]isoquinolin-2(3*H*)-yl)ethyl)-1*H*-1,2,3-triazol-4-yl)methyl)-1,4,8,11-tetraazacyclotetradecane-1,4,8-tricarboxylate (18). Propargyl-tri-Boc cyclam [23,36] (298 mg, 0.553 mmol) and azide **17** (193 mg, 0.552 mmol) were reacted at room temperature using general synthetic procedure A to give **18** as a

yellow foam (453 mg, 92%). **R_F** (EtOAc:hexane = 1:1) 0.19. **IR** $\nu_{\max}/\text{cm}^{-1}$ 2973, 2934, 2859, 2815, 1689, 1659, 1585, 1459, 1363, 1240, 1162, 1035, 864. **¹H NMR** (400 MHz, CDCl₃) δ 1.44 (s, 9H, C(CH₃)₃), 1.47 (s, 18H, 2 × C(CH₃)₃), 1.63–1.78 (m, 4H, CH₂CH₂CH₂CH₂CH₂ & NCH₂CH₂CH₂N), 1.83–1.99 (m, 6H, CH₂CH₂CH₂CH₂CH₂ & NCH₂CH₂CH₂N), 2.28–2.42 (m, 2H, CH₂N(CH₂-triazole)CH₂), 2.49–2.61 (m, 2H, CH₂N(CH₂-triazole)CH₂), 3.23 (t, 4H, *J* 5.2, CH₂N(naphthalene)CH₂), 3.18–3.52 (m, 12H, 3 × CH₂N(Boc)CH₂), 3.78 (s, 2H, NCH₂-triazole), 4.64 (t, 2H, *J* 6.0), 4.75 (t, 2H, *J* 6.0) (total 4H, triazole-CH₂CH₂N), 7.15 (d, 1H, *J* 8.4, naphthalene-H), 7.55 (br s, 1H, triazole-H), 7.64 (dd, 1H, *J* 8.4 & 7.2, naphthalene-H), 8.37 (dd, 1H, *J* 8.4 & 1.2, naphthalene-H), 8.40 (d, 1H, *J* 8.0, naphthalene-H), 8.47 (dd, 1H, *J* 7.6 & 1.2, naphthalene-H). **¹³C NMR** (100 MHz, CDCl₃) δ 24.3, 26.2, 26.6, 28.5, 28.6, 39.5, 45.2, 47.0, 47.9, 50.7, 51.7, 53.0, 54.5, 79.5, 114.7, 115.1, 122.5, 123.1, 125.3, 126.3, 130.1, 131.1, 131.3, 133.0, 143.0, 155.5, 155.8, 157.7, 163.7, 164.3 (seventeen carbon signals overlapping or obscured). **MS** (ESI) m/z 588.2 ([M-3Boc+H]⁺, 22%), 688.0 ([M-2Boc+H]⁺, 16%), 788.2 ([M-Boc+H]⁺, 31%), 888.2 ([M+H]⁺, 100%), 910.3 ([M+Na]⁺, 46%). **HRMS** (ESI) 910.51580 ([M+Na]⁺); calcd. for C₄₇H₆₉N₉NaO₈ ([M+Na]⁺) 910.51613.

2-(2-(4-((1,4,8,11-Tetraazacyclotetradecan-1-yl)methyl)-1H-1,2,3-triazol-1-yl)ethyl)-6-(piperidin-1-yl)-1H-benzo[de]isoquinoline-1,3(2H)-dione (9). Compound **18** (133 mg, 0.150 mmol) was deprotected using general synthetic procedure B to give **9** as a yellow glue (87 mg, 99%). **IR** $\nu_{\max}/\text{cm}^{-1}$ 3269, 2934, 2846, 2814, 1692, 1653, 1584, 1516, 1458, 1384, 1356, 1239, 1118, 1079, 1028. **¹H NMR** (400 MHz, CDCl₃) δ 1.50–2.00 (m, 10H, CH₂CH₂CH₂CH₂ & 2 × NCH₂CH₂CH₂N), 2.20–2.84 (m, 16H, 3 × CH₂NHCH₂ & CH₂N(CH₂-triazole)CH₂), 3.95–3.50 (m, 7H, 3 × CH₂NHCH₂ & CH₂N(naphthalene)CH₂), 3.69 (s, 2H, NCH₂-triazole), 4.54 (t, 2H, *J* 5.2), 4.65 (t, 2H, *J* 5.2) (total 4H, triazole-CH₂CH₂N), 7.04 (d, 1H, *J* 8.0, naphthalene-H), 7.54 (t, 1H, *J* 7.6, naphthalene-H), 7.60 (s, 1H, triazole-H), 8.26 (d, 1H, *J* 6.8, naphthalene-H), 8.28 (d, 1H, *J* 7.6, naphthalene-H), 8.36 (d, 1H, *J* 6.8, naphthalene-H). **¹³C NMR** (100 MHz, CDCl₃) δ 24.2, 25.7, 26.1, 28.4, 39.5, 46.7, 47.0, 47.6, 47.8, 48.6, 49.2, 50.7, 52.4, 54.0, 54.4, 114.6, 114.9, 122.3, 123.0, 125.2, 126.1, 129.9, 131.0, 131.1, 132.8, 143.9, 157.6, 163.5, 164.1 (three carbon signals overlapping or obscured). **MS** (ESI) m/z 588.2 ([M+H]⁺, 100%). **HRMS** (ESI) 588.37694 ([M+H]⁺); calcd. for C₃₂H₄₆N₉O₂ ([M+H]⁺) 588.37690.

6-(Piperidin-1-yl)-2-(4-((trimethylsilyl)ethynyl)phenyl)-1H-benzo[de]isoquinoline-1,3(2H)-dione (19) [32]. To a solution of **12** (1.31 g, 3.01 mmol), CuI (269 mg, 1.41 mmol), triphenylphosphine (1.06 g, 4.04 mmol) and Pd(PPh₃)₄ (263 mg, 0.228 mmol) in Et₃N (18 mL) were added pyridine (9 mL) and trimethylsilylacetylene (4.25 mL, 30.1 mmol). The reaction mixture was heated at 85 °C under Ar overnight and cooled to room temperature before addition of DCM (40 mL). The organic phase was washed with H₂O (4 × 40 mL), dried over MgSO₄ and concentrated under reduced pressure. The residue was purified by flash column chromatography (silica gel, DCM:hexane = 5:1) to give **19** as a yellow solid (1.28 g, 94%). **R_F** (DCM) 0.67. **m.p.** 258–259 °C. **IR** $\nu_{\max}/\text{cm}^{-1}$ 2959, 2926, 2854, 2794, 2364, 2332, 2156, 1707, 1658, 1590, 1508, 1453, 1401, 1376, 1237, 1196, 1148, 869, 838. **¹H NMR** (300 MHz, CDCl₃) δ 0.27 (s, 9H, Si(CH₃)₃), 1.65–1.80 (m, 2H, CH₂CH₂CH₂CH₂CH₂), 1.84–1.98 (m, 4H, CH₂CH₂CH₂CH₂CH₂), 3.25 (t, 4H, *J* 5.1, CH₂NCH₂), 7.18 (d, 1H, *J* 8.1, naphthalene-H), 7.24 (d, 2H, *J* 8.1, Ph-H), 7.61 (d, 2H, *J* 8.4, Ph-H), 7.69 (t, 1H, *J* 7.8, naphthalene-H), 8.43 (d, 1H, *J* 8.4, naphthalene-H), 8.50 (d, 1H, *J* 8.1, naphthalene-H), 8.58 (d, 1H, *J* 7.5, naphthalene-H). **¹³C NMR** (75 MHz, CDCl₃) δ 0.1, 24.4, 26.3, 54.6, 95.1, 104.7, 114.9, 115.8, 123.2, 123.6, 125.5, 126.4, 128.9, 130.4, 131.2, 131.5, 132.9, 133.2, 135.9, 157.8, 164.1, 164.6 (six

carbon signals overlapping or obscured). **HRMS** (ESI) 453.19960 ([M+H]⁺); calcd. for C₂₈H₂₉N₉O₂Si ([M+H]⁺) 453.19928.

2-(4-Ethynylphenyl)-6-(piperidin-1-yl)-1H-benzo[de]isoquinoline-1,3(2H)-dione (20) [32]. To a solution of **19** (78 mg, 0.17 mmol) in CH₃OH (5 mL) was added K₂CO₃ (95 mg, 0.69 mmol). The reaction mixture was stirred at room temperature overnight and filtered. The solids were washed with H₂O (3 × 5 mL), dried and purified by flash column chromatography (silica gel, DCM:hexane = 1:1 ramping to DCM) to give **20** as a yellow solid (63 mg, 97%). **R_F** (DCM:hexane = 5:1) 0.50. **m.p.** 263–264 °C. **IR** $\nu_{\max}/\text{cm}^{-1}$ 3254, 2943, 2917, 2850, 2807, 2361, 2331, 1696, 1647, 1585, 1508, 1449, 1372, 1233, 1187, 1138, 1077, 1034, 1000, 914, 832. **¹H NMR** (400 MHz, CDCl₃) δ 1.70–1.77 (m, 2H, CH₂CH₂CH₂CH₂CH₂), 1.87–1.94 (m, 4H, CH₂CH₂CH₂CH₂CH₂), 3.12 (s, 1H, C≡CH), 3.26 (t, 4H, *J* 5.2, CH₂NCH₂), 7.20 (d, 1H, *J* 8.0, naphthalene-H), 7.28 (d, 2H, *J* 8.4, Ph-H), 7.65 (d, 2H, *J* 8.4, Ph-H), 7.70 (t, 1H, *J* 8.0, naphthalene-H), 8.44 (d, 1H, *J* 8.4, naphthalene-H), 8.52 (d, 1H, *J* 8.0, naphthalene-H), 8.60 (d, 1H, *J* 7.2, naphthalene-H). **¹³C NMR** (75 MHz, CDCl₃) δ 24.5, 26.4, 54.7, 83.3, 114.9, 115.8, 122.6, 123.2, 125.6, 126.5, 129.1, 130.5, 131.3, 131.6, 133.2, 133.3, 136.3, 157.9, 164.2, 164.7 (five carbon signals overlapping or obscured). **HRMS** (ESI) 403.14150 ([M+Na]⁺); calcd. for C₂₅H₂₀N₂NaO₂ ([M+Na]⁺) 403.14170.

Tri-tert-butyl 11-(2-(4-(4-(1,3-dioxo-6-(piperidin-1-yl)-1H-benzo[de]isoquinolin-2(3H)-yl)phenyl)-1H-1,2,3-triazol-1-yl)ethyl)-1,4,8,11-tetraazacyclotetradecane-1,4,8-tricarboxylate (21). Azide **S3** (382 mg, 0.670 mmol) and alkyne **20** (255 mg, 0.670 mmol) were reacted at 50 °C using general synthetic procedure A to give **21** as a yellow foam (423 mg, 66%). **R_F** (EtOAc:hexane = 1:1) 0.17. **IR** $\nu_{\max}/\text{cm}^{-1}$ 2973, 2937, 2861, 2817, 1689, 1584, 1462, 1413, 1366, 1235, 1161, 1074. **¹H NMR** (300 MHz, CDCl₃) δ 1.46 (s, 9H, C(CH₃)₃), 1.47 (s, 18H, 2 × C(CH₃)₃), 1.62–1.85 (m, 6H, CH₂CH₂CH₂CH₂CH₂ & 2 × NCH₂CH₂CH₂N), 1.85–2.00 (m, 4H, CH₂CH₂CH₂CH₂CH₂), 2.46–2.62 (m, 2H, CH₂N(CH₂CH₂-triazole)CH₂), 2.62–2.79 (m, 2H, CH₂N(CH₂-triazole)CH₂), 2.92–3.10 (m, 2H, NCH₂CH₂-triazole), 3.10–3.50 (m, 16H, 3 × CH₂N(Boc)CH₂ & CH₂N(naphthalene)CH₂), 4.36–4.53 (m, 2H, NCH₂CH₂-triazole), 7.21 (d, 1H, *J* 8.1, naphthalene-H), 7.38 (d, 2H, *J* 8.1, Ph-H), 7.71 (t, 1H, *J* 7.8, naphthalene-H), 7.91 (br s, 1H, triazole-H), 8.01 (d, 2H, *J* 8.1, Ph-H), 8.45 (d, 1H, *J* 8.4, naphthalene-H), 8.53 (d, 1H, *J* 8.1, naphthalene-H), 8.61 (d, 1H, *J* 7.2, naphthalene-H). **¹³C NMR** (75 MHz, CDCl₃) δ 24.4, 26.3, 28.6, 45.9, 47.0, 47.5, 47.9, 48.3, 52.4, 53.5, 54.6, 55.1, 79.8, 79.9, 114.8, 115.9, 120.7, 123.3, 125.5, 126.4, 126.5, 129.4, 130.4, 130.9, 131.1, 131.5, 133.2, 135.6, 147.1, 155.6, 155.8, 157.7, 164.2, 164.8 (eighteen carbon signals overlapping or obscured). **MS** (ESI) m/z 972.2 ([M+Na]⁺, 100%). **HRMS** (ESI) 972.53168 ([M+Na]⁺); calcd. for C₅₂H₇₁N₉NaO₈ ([M+Na]⁺) 972.53178.

2-(4-(1-(2-(1,4,8,11-Tetraazacyclotetradecan-1-yl)ethyl)-1H-1,2,3-triazol-4-yl)phenyl)-6-(piperidin-1-yl)-1H-benzo[de]isoquinoline-1,3(2H)-dione (10). Compound **21** (143 mg, 0.150 mmol) was deprotected using general synthetic procedure B to give **10** as a yellow glue (97 mg, 99%). **IR** $\nu_{\max}/\text{cm}^{-1}$ 3282, 3056, 2933, 2814, 1700, 1659, 1582, 1509, 1457, 1363, 1230, 1188, 1134, 1076, 1045, 1000, 912, 830. **¹H NMR** (400 MHz, CDCl₃) δ 1.60–1.82 (m, 6H, CH₂CH₂CH₂CH₂CH₂ & 2 × NCH₂CH₂CH₂N), 1.82–2.00 (m, 4H, CH₂CH₂CH₂CH₂CH₂), 2.20–2.85 (m, 19H, 3 × CH₂NHCH₂ & CH₂N(CH₂CH₂-triazole)CH₂), 2.94 (t, 2H, *J* 6.0, NCH₂CH₂-triazole), 3.12–3.42 (m, 4H, CH₂N(naphthalene)CH₂), 4.57 (t, 2H, *J* 6.0, NCH₂CH₂-triazole), 7.19 (d, 1H, *J* 8.0, naphthalene-H), 7.37 (d, 2H, *J* 8.4, Ph-H), 7.69 (t, 1H, *J* 8.0, naphthalene-H), 8.01 (d, 2H, *J* 8.0, Ph-H), 8.20 (s, 1H, triazole-H), 8.43 (d, 1H, *J* 8.4, naphthalene-H), 8.50 (d, 1H, *J* 8.0, naphthalene-

H), 8.58 (d, 1H, J 6.8, naphthalene-H). ^{13}C NMR (100 MHz, CDCl_3) δ 24.3, 26.1, 28.5, 46.7, 47.2, 47.6, 48.3, 48.6, 50.7, 51.2, 52.9, 54.4, 54.6, 114.7, 115.7, 121.7, 123.1, 125.3, 126.3, 129.3, 130.3, 130.9, 131.0, 131.3, 132.9, 135.5, 146.5, 157.5, 164.0, 164.5 (seven carbon signals overlapping or obscured). MS (ESI) m/z 650.2 ($[\text{M}+\text{H}]^+$, 100%), 1299.1 ($[\text{2M}+\text{H}]^+$, 30%). HRMS (ESI) 650.39253 ($[\text{M}+\text{H}]^+$); calcd. for $\text{C}_{37}\text{H}_{48}\text{N}_9\text{O}_2$ ($[\text{M}+\text{H}]^+$) 650.39255.

(d) Photophysical Studies

All UV-Vis and fluorescence experiments were performed with a 1 cm fluorescence quartz cuvette. For metal ion binding studies, a small amount (2–10 μL) of a solution of metal perchlorate (2–10 mM in metal) in HEPES buffer (10 mM, pH 7.4) was added to a solution of **8–10** (10 μM , 2 mL) in HEPES buffer (10 mM, pH 7.4). For competitive binding studies, 50 equivalents of Zn^{2+} or Cu^{2+} were added to a 10 μM solution of **8–10** in HEPES buffer (10 mM, pH 7.4), followed after approximately 3 min by addition of 1 equivalent of Cu^{2+} or Zn^{2+} respectively; a premixed $\text{Cu}^{2+}/\text{Zn}^{2+}$ (1 equivalent/50 equivalents) solution was added to a 10 μM solution of **8–10** in HEPES buffer (10 mM, pH 7.4). For pH studies, the pH value of a solution of **8–10** (10 μM , 2 mL) in HEPES buffer (10 mM, pH 7.4) was adjusted with either 1 M HClO_4 or 1 M NaOH prior to addition of Cu^{2+} . For the solvent studies, solutions of **8–10** (1–2 μM , 2 mL) were prepared in different solvents. For the quantum yield and time resolved measurements in HEPES-buffer, ethyl acetate and MeCN, solutions were prepared freshly and the absorbance was adjusted to 0.1.

(e) Cell Viability Assay

The cytotoxicity of compounds **8–10**, **14**, **18** and **21** was evaluated using cell viability assay as described previously. [50] Compounds **8–10**, **14**, **18** and **21** were prepared as a 10 mM stock solution in DMSO and diluted with growth medium (2% FCS and 1% glutamine) to give rise to a range of concentrations (0–200 μM). DLD-1 colon carcinoma cells and MDA-MB-231 breast carcinoma cells were cultured as monolayers in Advanced DMEM, supplemented with 2% FCS, 1% glutamine and 1% antibiotic/antimycotic (A/A). Cells were incubated at 37°C with 5% CO_2 in a humidified incubator, seeded at 1×10^4 cells per well of a 96-well plate in 100 μL of growth medium, and allowed to adhere for 15 h. Growth medium was removed, and 100 μL of compounds at different concentrations were added in triplicate. The plates were incubated for 72 h. 3-(4,5-Dimethylthiazol-2-yl)-2,5-diphenyltetrazolium bromide (MTT, 20 μL), a water-aqueous soluble yellow tetrazole compound, was added to a final concentration of 1 mM per well and the plates were incubated for 4 h. Growth medium was removed, and DMSO (150 μL) was added to dissolve the water-insoluble purple formazan crystals. The plates were shaken until all the crystals were dissolved. The absorbances at 600 nm were read by a microplate reader (Victor, PerkinElmer) and averaged for each concentration. IC_{50} value was determined by the concentration of the compound at which the absorbance was half of that of the cells grown in only growth medium. The average of three independent IC_{50} values for each concentration was used to calculate the standard error of the mean.

Supporting Information

File S1 File S1 Contains the files: Text S1. Lippert-Mataga Equation. Text S2. Synthesis of Known Compounds. **Figure S1.** Stokes shift (λ) of **8** versus orientation polarizability (Δf). The red, straight line represents the best

linear fit to the 13 data points [coefficient of determination $R^2 = 0.560$, slope = $(4.32 \pm 1.07) \times 10^3 \text{ cm}^{-1}$, intercept = $(4.41 \pm 0.26) \times 10^3 \text{ cm}^{-1}$]. **Figure S2.** Stokes shift (λ) of **9** versus orientation polarizability (Δf). The red, straight line represents the best linear fit to the 13 data points [coefficient of determination $R^2 = 0.392$, slope = $(3.00 \pm 1.02) \times 10^3 \text{ cm}^{-1}$, intercept = $(4.61 \pm 0.25) \times 10^3 \text{ cm}^{-1}$]. **Figure S3.** Stokes shift (λ) of **10** versus orientation polarizability (Δf). The red, straight line represents the best linear fit to the 13 data points [coefficient of determination $R^2 = 0.562$, slope = $(4.07 \pm 1.00) \times 10^3 \text{ cm}^{-1}$, intercept = $(4.53 \pm 0.25) \times 10^3 \text{ cm}^{-1}$]. **Figure S4.** Fluorescence spectra of **8** (10 μM) in the presence of various metal ions. Experiments were carried out in HEPES buffer (10 mM, pH 7.4) at 25°C and the fluorescence emission spectra were recorded about 5 min after addition of various metal ions (1 equiv.). **Figure S5.** Fluorescence spectra of **9** (10 μM) in the presence of various metal ions. Experiments were carried out in HEPES buffer (10 mM, pH 7.4) at 25°C and the fluorescence emission spectra were recorded about 5 min after addition of various metal ions (1 equiv.). **Figure S6.** Fluorescence spectra of **10** (10 μM) in the presence of various metal ions. Experiments were carried out in HEPES buffer (10 mM, pH 7.4) at 25°C and the fluorescence emission spectra were recorded about 5 min after addition of various metal ions (1 equiv.). **Figure S7.** UV-Vis spectra of **8** (10 μM) in the presence of various metal ions. Experiments were carried out in HEPES buffer (10 mM, pH 7.4) at 25°C and the UV-Vis spectra were recorded about 5 min after addition of various metal ions (1 equiv.). **Figure S8.** UV-Vis spectra of **9** (10 μM) in the presence of various metal ions. Experiments were carried out in HEPES buffer (10 mM, pH 7.4) at 25°C and the UV-Vis spectra were recorded about 5 min after addition of various metal ions (1 equiv.). **Figure S9.** UV-Vis spectra of **10** (10 μM) in the presence of various metal ions. Experiments were carried out in HEPES buffer (10 mM, pH 7.4) at 25°C and the UV-Vis spectra were recorded about 5 min after addition of various metal ions (1 equiv.). **Figure S10.** Fluorescence emission of **8** (10 μM) in the absence and presence of Cu^{2+} (1 equiv.) over a range of pH values. Experiments were carried out in HEPES buffer (10 mM, pH 7.4) at 25°C. **Figure S11.** Fluorescence emission of **9** (10 μM) in the absence and presence of Cu^{2+} (1 equiv.) over a range of pH values. Experiments were carried out in HEPES buffer (10 mM, pH 7.4) at 25°C. **Figure S12.** Fluorescence emission of **10** (10 μM) in the absence and presence of Cu^{2+} (1 equiv.) over a range of pH values. Experiments were carried out in HEPES buffer (10 mM, pH 7.4) at 25°C. **Figure S13.** Synthesis of 2-azidoethyl-tri-Boc cyclam **S3**. Reagents and conditions: (a) (i) NaN_3 , H_2O , reflux, o/n; (ii) *p*-toluenesulfonyl chloride, Et_3N , rt, 6 h; (iii) glycine, rt, 2 h, 65%; (b) tri-Boc cyclam, Na_2CO_3 , CH_3CN , reflux, 96 h, 66%. **Figure S14.** Synthesis of compound **12**. Reagents and conditions: (a) piperidine, 2-methoxyethanol, reflux, 36 h, 86%; (b) 4-bromoaniline, piperidine, 2-methoxyethanol, reflux, 72 h, 90%. **Figure S15.** Synthesis of compound **17**. Reagents and conditions: (a) 2-aminoethanol, EtOH , reflux, 22 h, 92%; (b) PBr_3 , pyridine, THF, 50°C, 16 h, 60%; (c) NaN_3 , EtOH , reflux, 6 h, 80%. **Figure S16.** ^1H NMR spectrum (300 MHz) of **13** in CDCl_3 . **Figure S17.** ^{13}C NMR spectrum (75 MHz) of **13** in CDCl_3 . **Figure S18.** ^1H NMR spectrum (300 MHz) of **14** in CDCl_3 . **Figure S19.** ^{13}C NMR spectrum (75 MHz) of **14** in CDCl_3 . **Figure S20.** ^1H NMR spectrum (400 MHz) of **8** in CDCl_3 . **Figure S21.** ^{13}C NMR spectrum (100 MHz) of **8** in CDCl_3 . **Figure S22.** ^1H NMR spectrum (400 MHz) of **18** in

CDCl₃. Figure S23. ¹³C NMR spectrum (100 MHz) of 18 in CDCl₃. Figure S24. ¹H NMR spectrum (400 MHz) of 9 in CDCl₃. Figure S25. ¹³C NMR spectrum (100 MHz) of 9 in CDCl₃. Figure S26. ¹H NMR spectrum (300 MHz) of 19 in CDCl₃. Figure S27. ¹³C NMR spectrum (75 MHz) of 19 in CDCl₃. Figure S28. ¹H NMR spectrum (400 MHz) of 20 in CDCl₃. Figure S29. ¹³C NMR spectrum (75 MHz) of 20 in CDCl₃. Figure S30. ¹H NMR spectrum (300 MHz) of 21 in CDCl₃. Figure S31. ¹³C NMR spectrum (75 MHz) of 21 in CDCl₃. Figure S32. ¹H

NMR spectrum (400 MHz) of 10 in CDCl₃. Figure S33. ¹³C NMR spectrum (100 MHz) of 10 in CDCl₃. (ZIP)

Author Contributions

Conceived and designed the experiments: MY SA QY ATSL RF PJR MHT. Performed the experiments: MY SA QY ATSL RF. Analyzed the data: MY SA QY ATSL RF PJR MHT. Contributed reagents/materials/analysis tools: MY SA QY ATSL RF. Wrote the paper: MY SA PJR MHT.

References

- Hyman LM, Franz KJ (2012) Probing oxidative stress: small molecule fluorescent sensors of metal ions, reactive oxygen species, and thiols. *Coord Chem Rev* 256: 2333–2356.
- Yang Y, Zhao Q, Feng W, Li F (2013) Luminescent chemodosimeters for bioimaging. *Chem Rev* 113: 192–270.
- Grabchev I, Staneva D, Betecheva R (2012) Fluorescent dendrimers as sensors for biologically important metal cations. *Curr Med Chem* 19: 4976–4983.
- Mbatia HW, Burdette SC (2012) Photochemical tools for studying metal ion signaling and homeostasis. *Biochemistry* 51: 7212–7224.
- Dean KM, Qin Y, Palmer AE (2012) Visualizing metal ions in cells: an overview of analytical techniques, approaches, and probes. *BBA-Mol Cell Res* 1823: 1406–1415.
- Schäferling M (2012) The art of fluorescence imaging with chemical sensors. *Angew Chem Int Ed* 51: 3532–3554.
- Jeong Y, Yoon J (2012) Recent progress on fluorescent chemosensors for metal ions. *Inorg Chim Acta* 381: 2–14.
- Fegley MEA, Pinnock SS, Malele CN, Jones Jr WE (2012) Metal-containing conjugated polymers as fluorescent chemosensors in the detection of toxicants. *Inorg Chim Acta* 381: 78–84.
- Xu Z, Xiao Y, Qian X, Cui J, Cui D (2005) Ratiometric and selective fluorescent sensor for Cu(II) based on internal charge transfer (ICT). *Org Lett* 7: 889–892.
- Xu Z, Qian X, Cui J (2005) Colorimetric and ratiometric fluorescent chemosensor with a large red-shift in emission: Cu(II)-only sensing by deprotonation of secondary amines as receptor conjugated to naphthalimide fluorophore. *Org Lett* 7: 3029–3032.
- Huang J, Xu Y, Qian X (2009) A red-shift colorimetric and fluorescent sensor for Cu²⁺ in aqueous solution: unsymmetrical 4,5-diaminonaphthalimide with N-H deprotonation induced by metal ions. *Org Biomol Chem* 7: 1299–1303.
- Singh N, Kaur N, McCaughan B, Callan JF (2010) Ratiometric fluorescent detection of Cu(II) in semi-aqueous solution using a two-fluorophore approach. *Tetrahedron Lett* 51: 3385–3387.
- Xu Z, Pan J, Spring DR, Cui J, Yoon J (2010) Ratiometric fluorescent and colorimetric sensors for Cu²⁺ based on 4,5-disubstituted-1,8-naphthalimide and sensing cyanide *via* Cu²⁺ displacement approach. *Tetrahedron* 66: 1678–1683.
- Xu Z, Kim S, Kim HN, Han SJ, Lee C, et al. (2007) A naphthalimide-calixarene as a two-faced and highly selective fluorescent chemosensor for Cu²⁺ or F⁻. *Tetrahedron Lett* 48: 9151–9154.
- Xu H, Zeng X, Dai H (2011) A new fluorescent chemosensor for metal ions based upon 1,8-naphthalimide and 8-hydroxyquinoline. *Chin J Chem* 29: 2165–2168.
- Dai H, Xu H (2012) Selective and sensitive fluorescent chemosensors for Cu²⁺ ion based upon bis-1,8-naphthalimide dyads. *Chin J Chem* 30: 267–272.
- Dai H, Yan Y, Guo Y, Fan L, Che Z, et al. (2012) A selective and sensitive “turn-on” fluorescent chemosensor for recognition of Hg²⁺ ions in water. *Chem Eur J* 18: 11188–11191.
- Dai H, Xu H (2011) A water-soluble 1,8-naphthalimide-based ‘turn on’ fluorescent chemosensor for selective and sensitive recognition of mercury ion in water. *Bioorg Med Chem Lett* 21: 5141–5144.
- Jobe K, Brennan CH, Motevalli M, Goldup SM, Watkinson M (2011) Modular ‘click’ sensors for zinc and their application *in vivo*. *Chem Commun* 47: 6036–6038.
- Tamanini E, Flavin K, Motevalli M, Piperno S, Gheber LA, et al. (2010) Cyclam-based “clickates”: homogeneous and heterogeneous fluorescent sensors for Zn(II). *Inorg Chem* 49: 3789–3800.
- Tamanini E, Katewa A, Sedger LM, Todd MH, Watkinson M (2009) A synthetically simple, click-generated cyclam-based zinc(II) sensor. *Inorg Chem* 48: 319–324.
- Ast S, Rutledge PJ, Todd MH (2012) Reversing the triazole topology in a cyclam-triazole-dye ligand gives a 10-fold brighter signal response to Zn²⁺ in aqueous solution. *Eur J Inorg Chem* 2012: 5611–5615.
- Yu M, Yu Q, Rutledge PJ, Todd MH (2013) A fluorescent “allosteric scorpionand” complex visualizes a biological recognition event. *ChemBioChem* 14: 224–229.
- Lau YH, Price JR, Todd MH, Rutledge PJ (2011) A click fluorophore sensor that can distinguish Cu^{II} and Hg^{II} *via* selective anion-induced demetallation. *Chem Eur J* 17: 2850–2858.
- Kronick MN, Grossman PD (1983) Immunoassay techniques with fluorescent phycobiliprotein conjugates. *Clin Chem* 29: 1582–1586.
- Parkesh R, Clive Lee T, Gunnlaugsson T (2007) Highly selective 4-amino-1,8-naphthalimide based fluorescent photoinduced electron transfer (PET) chemosensors for Zn(II) under physiological pH conditions. *Org Biomol Chem* 5: 310–317.
- Gunnlaugsson T, Kruger PE, Lee TC, Parkesh R, Pfeffer FM, et al. (2003) Dual responsive chemosensors for anions: the combination of fluorescent PET (Photoinduced Electron Transfer) and colorimetric chemosensors in a single molecule. *Tetrahedron Lett* 44: 6575–6578.
- Mednykh YA, Manaev YA, Volchikov VV, Uzhinov BM (2004) Influence of the configuration of the amine nitrogen atom on the efficiency of fluorescence of 4-aminonaphthalimide derivatives. *Russ J Gen Chem* 74: 1728–1733.
- Ding G, Xu Z, Zhong G, Jing S, Li F, et al. (2008) Synthesis, photophysical and electrochromic properties of novel naphthalimide derivatives containing an electron-transporting unit. *Res Chem Intermed* 34: 299–308.
- Wang D, Zhang X, He C, Duan C (2010) Aminonaphthalimide-based imidazolium podands for turn-on fluorescence sensing of nucleoside polyphosphates. *Org Biomol Chem* 8: 2923–2925.
- Tagg T, McAdam CJ, Robinson BH, Simpson J (2008) *N*-(2-Bromoethyl)-4-piperidino-1,8-naphthalimide and *N*-(3-bromopropyl)-4-piperidino-1,8-naphthalimide. *Acta Crystallogr C* 64: o388–o391.
- Baier MC, Huber J, Mecking S (2009) Fluorescent conjugated polymer nanoparticles by polymerization in miniemulsion. *J Am Chem Soc* 131: 14267–14273.
- Markiewicz JT, Wiest O, Helquist P (2010) Synthesis of primary aryl amines through a copper-assisted aromatic substitution reaction with sodium azide. *J Org Chem* 75: 4887–4890.
- Zhu W, Ma D (2004) Synthesis of aryl azides and vinyl azides *via* proline-promoted Cu^I-catalyzed coupling reactions. *Chem Commun*: 888–889.
- Andersen J, Madsen U, Björklund F, Liang X (2005) Rapid synthesis of aryl azides from aryl halides under mild conditions. *Synlett* 2005: 2209–2213.
- Yu M, Price JR, Jensen P, Lovitt CJ, Shelper T, et al. (2011) Copper, nickel, and zinc cyclam-amino acid and cyclam-peptide complexes may be synthesized with “click” chemistry and are nontoxic. *Inorg Chem* 50: 12823–12835.
- Yu M, Lim NH, Ellis S, Nagase H, Triccas JA, et al. (2013) Incorporation of bulky and cationic cyclam-triazole moieties into marimastat can generate potent MMP inhibitory activity without inducing cytotoxicity. *ChemistryOpen* 2: 99–105.
- Tamanini E, Rigby SEJ, Motevalli M, Todd MH, Watkinson M (2009) Responsive metal complexes: a click-based “allosteric scorpionate” complex permits the detection of a biological recognition event by EPR/ENDOR spectroscopy. *Chem Eur J* 15: 3720–3728.
- Lippert E (1955) Dipolmoment und elektronenstruktur von angeregten molekülen. *Z Naturforsch, A: Phys Sci* 10: 541–545.
- Mataga N, Kaifu Y, Koizumi M (1955) The solvent effect on fluorescence spectrum, change of solute-solvent interaction during the lifetime of excited solute molecule. *Bull Chem Soc Jpn* 28: 690–691.
- Mataga N, Kaifu Y, Koizumi M (1956) Solvent effects upon fluorescence spectra and the dipolemoments of excited molecules. *Bull Chem Soc Jpn* 29: 465–470.
- Filarowski A, Kluba M, Cieslik-Bocuzla K, Koll A, Kochel A, et al. (2010) Generalized solvent scales as a tool for investigating solvent dependence of spectroscopic and kinetic parameters. Application to fluorescent BODIPY dyes. *Photochem Photobiol Sci* 9: 996–1008.
- Werner TC, Hoffman RM (1973) Relation between an excited state geometry change and the solvent dependence of 9-methyl anthroate fluorescence. *J Phys Chem* 77: 1611–1615.
- McClure DS (1952) Spin-orbit interaction in aromatic molecules. *J Chem Phys* 20: 682–686.
- Varnes AW, Dodson RB, Wehry EL (1972) Interactions of transition-metal ions with photoexcited states of flavines. Fluorescence quenching studies. *J Am Chem Soc* 94: 946–950.
- Masuhara H, Shioyama H, Saito T, Hamada K, Yasoshima S, et al. (1984) Fluorescence quenching mechanism of aromatic hydrocarbons by closed-shell heavy metal ions in aqueous and organic solutions. *J Phys Chem* 88: 5868–5873.
- De Costa MDP, Jayasinghe WAPA (2004) Detailed studies on complexation behaviour and mechanism of fluorescence quenching of naphthalene linked

- hydroxamic acid with transition metal ions by UV-visible and fluorescence spectra. *J Photochem Photobiol, A* 162: 591–598.
48. de Silva AP, Gunaratne HQN, Habib-Jiwan J-L, McCoy CP, Rice TE, et al. (1995) New fluorescent model compounds for the study of photoinduced electron transfer: the influence of a molecular electric field in the excited state. *Angew Chem Int Ed* 34: 1728–1731.
 49. Zhang JZ, Bryce NS, Lanzirotti A, Chen CKJ, Paterson D, et al. (2012) Getting to the core of platinum drug bio-distributions: the penetration of anti-cancer platinum complexes into spheroid tumour models. *Metallomics* 4: 1209–1217.
 50. Kim BJ, Hambley TW, Bryce NS (2011) Visualising the hypoxia selectivity of cobalt(III) prodrugs. *Chem Sci* 2: 2135–2142.